

breco-06/11
BAD 2050, version 13

Collaboration-Wide Review

18 May 2009 to 1 June 2009

Primary BAD	2050, version 13 Measurement of CP observables for the decays $B^{+/-} \rightarrow DK^{*+/-}$
Author list	Benelli, Gabriele; Kass, Richard; Rahimi, Amir; Tisserand, Vincent; Wong, Quincy K.
Review Committee	comm371, members: Kolomensky, Yury; Soffer, Abi; Swain, Sanjay (chair)
Target	Physical Review D
Result type	
Supporting BAD(s)	BAD #1719 Analysis of B^- to $D^0 K^{*-}$ decays using GLW and ADS methods
Changes since preliminary result	
BAIS/CWR Comments	
Institutional Reading Groups	2a. Imperial College, Iowa, LBNL, Maryland, Padova, Rostock 2b. Budker, UCLA, Colorado, Royal Holloway, McGill, MIT, Trieste

Measurement of CP violation observables and parameters for the decays $B^\pm \rightarrow DK^{*\pm}$

B. Aubert,¹ Y. Karyotakis,¹ J. P. Lees,¹ V. Poireau,¹ E. Prencipe,¹ X. Prudent,¹ V. Tisserand,¹ J. Garra Tico,²
 E. Grauges,² M. Martinelli^{ab,3} A. Palano^{ab,3} M. Pappagallo^{ab,3} G. Eigen,⁴ B. Stugu,⁴ L. Sun,⁴ M. Battaglia,⁵
 D. N. Brown,⁵ L. T. Kerth,⁵ Yu. G. Kolomensky,⁵ G. Lynch,⁵ I. L. Osipenkov,⁵ K. Tackmann,⁵ T. Tanabe,⁵
 C. M. Hawkes,⁶ N. Soni,⁶ A. T. Watson,⁶ H. Koch,⁷ T. Schroeder,⁷ D. J. Asgeirsson,⁸ B. G. Fulsom,⁸ C. Hearty,⁸
 T. S. Mattison,⁸ J. A. McKenna,⁸ M. Barrett,⁹ A. Khan,⁹ A. Randle-Conde,⁹ V. E. Blinov,¹⁰ A. D. Bukin,^{10,*}
 A. R. Buzykaev,¹⁰ V. P. Druzhinin,¹⁰ V. B. Golubev,¹⁰ A. P. Onuchin,¹⁰ S. I. Serednyakov,¹⁰ Yu. I. Skovpen,¹⁰
 E. P. Solodov,¹⁰ K. Yu. Todyshev,¹⁰ M. Bondioli,¹¹ S. Curry,¹¹ I. Eschrich,¹¹ D. Kirkby,¹¹ A. J. Lankford,¹¹
 P. Lund,¹¹ M. Mandelkern,¹¹ E. C. Martin,¹¹ D. P. Stoker,¹¹ H. Atmacan,¹² J. W. Gary,¹² F. Liu,¹² O. Long,¹²
 G. M. Vitug,¹² Z. Yasin,¹² V. Sharma,¹³ C. Campagnari,¹⁴ T. M. Hong,¹⁴ D. Kovalskyi,¹⁴ M. A. Mazur,¹⁴
 J. D. Richman,¹⁴ T. W. Beck,¹⁵ A. M. Eisner,¹⁵ C. A. Heusch,¹⁵ J. Kroseberg,¹⁵ W. S. Lockman,¹⁵ A. J. Martinez,¹⁵
 T. Schalk,¹⁵ B. A. Schumm,¹⁵ A. Seiden,¹⁵ L. Wang,¹⁵ L. O. Winstrom,¹⁵ C. H. Cheng,¹⁶ D. A. Doll,¹⁶
 B. Echenard,¹⁶ F. Fang,¹⁶ D. G. Hitlin,¹⁶ I. Narsky,¹⁶ P. Ongmongkolku,¹⁶ T. Piatenko,¹⁶ F. C. Porter,¹⁶
 R. Andreassen,¹⁷ G. Mancinelli,¹⁷ B. T. Meadows,¹⁷ K. Mishra,¹⁷ M. D. Sokoloff,¹⁷ P. C. Bloom,¹⁸ W. T. Ford,¹⁸
 A. Gaz,¹⁸ J. F. Hirschauer,¹⁸ M. Nagel,¹⁸ U. Nauenberg,¹⁸ J. G. Smith,¹⁸ S. R. Wagner,¹⁸ R. Ayad,^{19,†}
 W. H. Toki,¹⁹ R. J. Wilson,¹⁹ E. Feltresi,²⁰ A. Hauke,²⁰ H. Jasper,²⁰ T. M. Karbach,²⁰ J. Merkel,²⁰ A. Petzold,²⁰
 B. Spaan,²⁰ K. Wacker,²⁰ M. J. Kobel,²¹ R. Nogowski,²¹ K. R. Schubert,²¹ R. Schwierz,²¹ D. Bernard,²²
 E. Latour,²² M. Verderi,²² P. J. Clark,²³ S. Playfer,²³ J. E. Watson,²³ M. Andreotti^{ab,24} D. Bettoni^{a,24} C. Bozzi^{a,24}
 R. Calabrese^{ab,24} A. Cecchi^{ab,24} G. Cibinetto^{ab,24} E. Fioravanti^{ab,24} P. Franchini^{ab,24} E. Luppi^{ab,24}
 M. Menerato^{ab,24} M. Negrini^{ab,24} A. Petrella^{ab,24} L. Piemontese^{a,24} V. Santoro^{ab,24} R. Baldini-Ferroli,²⁵
 A. Calcaterra,²⁵ R. de Sangro,²⁵ G. Finocchiaro,²⁵ S. Pacetti,²⁵ P. Patteri,²⁵ I. M. Peruzzi,^{25,‡} M. Piccolo,²⁵
 M. Rama,²⁵ A. Zallo,²⁵ R. Contri^{ab,26} E. Guido,²⁶ M. Lo Vetere^{ab,26} M. R. Monge^{ab,26} S. Passaggio^{a,26}
 C. Patrignani^{ab,26} E. Robutti^{a,26} S. Tosi^{ab,26} K. S. Chaisanguanthum,²⁷ M. Morii,²⁷ A. Adametz,²⁸ J. Marks,²⁸
 S. Schenk,²⁸ U. Uwer,²⁸ F. U. Bernlochner,²⁹ V. Klose,²⁹ H. M. Lacker,²⁹ T. Lueck,²⁹ A. Volk,²⁹ D. J. Bard,³⁰
 P. D. Dauncey,³⁰ M. Tibbetts,³⁰ P. K. Behera,³¹ M. J. Charles,³¹ U. Mallik,³¹ J. Cochran,³² H. B. Crawley,³²
 L. Dong,³² V. Eyges,³² W. T. Meyer,³² S. Prell,³² E. I. Rosenberg,³² A. E. Rubin,³² Y. Y. Gao,³³ A. V. Gritsan,³³
 Z. J. Guo,³³ N. Arnaud,³⁴ J. Béquilleux,³⁴ A. D’Orazio,³⁴ M. Davier,³⁴ D. Derkach,³⁴ J. Firmino da Costa,³⁴
 G. Grosdidier,³⁴ F. Le Diberder,³⁴ V. Lepeltier,³⁴ A. M. Lutz,³⁴ B. Malaescu,³⁴ S. Pruvot,³⁴ P. Roudeau,³⁴
 M. H. Schune,³⁴ J. Serrano,³⁴ V. Sordini,^{34,§} A. Stocchi,³⁴ G. Wormser,³⁴ D. J. Lange,³⁵ D. M. Wright,³⁵
 I. Bingham,³⁶ J. P. Burke,³⁶ C. A. Chavez,³⁶ J. R. Fry,³⁶ E. Gabathuler,³⁶ R. Gamet,³⁶ D. E. Hutchcroft,³⁶
 D. J. Payne,³⁶ C. Touramanis,³⁶ A. J. Bevan,³⁷ C. K. Clarke,³⁷ F. Di Lodovico,³⁷ R. Sacco,³⁷ M. Sigamani,³⁷
 G. Cowan,³⁸ S. Paramesvaran,³⁸ A. C. Wren,³⁸ D. N. Brown,³⁹ C. L. Davis,³⁹ A. G. Denig,⁴⁰ M. Fritsch,⁴⁰
 W. Gradl,⁴⁰ A. Hafner,⁴⁰ K. E. Alwyn,⁴¹ D. Bailey,⁴¹ R. J. Barlow,⁴¹ G. Jackson,⁴¹ G. D. Lafferty,⁴¹ T. J. West,⁴¹
 J. I. Yi,⁴¹ J. Anderson,⁴² C. Chen,⁴² A. Jawahery,⁴² D. A. Roberts,⁴² G. Simi,⁴² J. M. Tuggle,⁴² C. Dallapiccola,⁴³
 E. Salvati,⁴³ R. Cowan,⁴⁴ D. Dujmic,⁴⁴ P. H. Fisher,⁴⁴ S. W. Henderson,⁴⁴ G. Sciolla,⁴⁴ M. Spitznagel,⁴⁴
 R. K. Yamamoto,⁴⁴ M. Zhao,⁴⁴ P. M. Patel,⁴⁵ S. H. Robertson,⁴⁵ M. Schram,⁴⁵ P. Biassoni^{ab,46} A. Lazzaro^{ab,46}
 V. Lombardo^{a,46} F. Palombo^{ab,46} S. Stracka^{ab,46} L. Cremaldi,⁴⁷ R. Godang,^{47,¶} R. Kroeger,⁴⁷ P. Sonnek,⁴⁷
 D. J. Summers,⁴⁷ H. W. Zhao,⁴⁷ M. Simard,⁴⁸ P. Taras,⁴⁸ H. Nicholson,⁴⁹ G. De Nardo^{ab,50} L. Lista^{a,50}
 D. Monorchio^{ab,50} G. Onorato^{ab,50} C. Sciacca^{ab,50} G. Raven,⁵¹ H. L. Snoek,⁵¹ C. P. Jessop,⁵² K. J. Knoepfel,⁵²
 J. M. LoSecco,⁵² W. F. Wang,⁵² L. A. Corwin,⁵³ K. Honscheid,⁵³ H. Kagan,⁵³ R. Kass,⁵³ J. P. Morris,⁵³
 A. M. Rahimi,⁵³ S. J. Sekula,⁵³ Q. K. Wong,⁵³ N. L. Blount,⁵⁴ J. Brau,⁵⁴ R. Frey,⁵⁴ O. Igonkina,⁵⁴ J. A. Kolb,⁵⁴
 M. Lu,⁵⁴ R. Rahmat,⁵⁴ N. B. Sinev,⁵⁴ D. Strom,⁵⁴ J. Strube,⁵⁴ E. Torrence,⁵⁴ G. Castelli^{ab,55} N. Gagliardi^{ab,55}
 M. Margoni^{ab,55} M. Morandin^{a,55} M. Posocco^{a,55} M. Rotondo^{a,55} F. Simonetto^{ab,55} R. Stroili^{ab,55} C. Voci^{ab,55}
 P. del Amo Sanchez,⁵⁶ E. Ben-Haim,⁵⁶ G. R. Bonneaud,⁵⁶ H. Briand,⁵⁶ J. Chauveau,⁵⁶ O. Hamon,⁵⁶ Ph. Leruste,⁵⁶
 G. Marchiori,⁵⁶ J. Ocariz,⁵⁶ A. Perez,⁵⁶ J. Prendki,⁵⁶ S. Sitt,⁵⁶ L. Gladney,⁵⁷ M. Biasini^{ab,58} E. Manoni^{ab,58}
 C. Angelini^{ab,59} G. Batignani^{ab,59} S. Bettarini^{ab,59} G. Calderini^{ab,59,**} M. Carpinelli^{ab,59,††} A. Cervelli^{ab,59}
 F. Forti^{ab,59} M. A. Giorgi^{ab,59} A. Lusiani^{ac,59} M. Morganti^{ab,59} N. Neri^{ab,59} E. Paoloni^{ab,59} G. Rizzo^{ab,59}
 J. J. Walsh^{a,59} D. Lopes Pegna,⁶⁰ C. Lu,⁶⁰ J. Olsen,⁶⁰ A. J. S. Smith,⁶⁰ A. V. Telnov,⁶⁰ F. Anulli^{a,61}
 E. Baracchini^{ab,61} G. Cavoto^{a,61} R. Faccini^{ab,61} F. Ferrarotto^{a,61} F. Ferroni^{ab,61} M. Gaspero^{ab,61} P. D. Jackson^{a,61}
 L. Li Gioi^{a,61} M. A. Mazzoni^{a,61} S. Morganti^{a,61} G. Piredda^{a,61} F. Renga^{ab,61} C. Voena^{a,61} M. Ebert,⁶²
 T. Hartmann,⁶² H. Schröder,⁶² R. Waldi,⁶² T. Adye,⁶³ B. Franek,⁶³ E. O. Olaiya,⁶³ F. F. Wilson,⁶³

S. Emery,⁶⁴ L. Esteve,⁶⁴ G. Hamel de Monchenault,⁶⁴ W. Kozanecki,⁶⁴ G. Vasseur,⁶⁴ Ch. Yèche,⁶⁴ M. Zito,⁶⁴ M. T. Allen,⁶⁵ D. Aston,⁶⁵ R. Bartoldus,⁶⁵ J. F. Benitez,⁶⁵ R. Cenci,⁶⁵ J. P. Coleman,⁶⁵ M. R. Convery,⁶⁵ J. C. Dingfelder,⁶⁵ J. Dorfan,⁶⁵ G. P. Dubois-Felsmann,⁶⁵ W. Dunwoodie,⁶⁵ R. C. Field,⁶⁵ M. Franco Sevilla,⁶⁵ A. M. Gabareen,⁶⁵ M. T. Graham,⁶⁵ P. Grenier,⁶⁵ C. Hast,⁶⁵ W. R. Innes,⁶⁵ J. Kaminski,⁶⁵ M. H. Kelsey,⁶⁵ H. Kim,⁶⁵ P. Kim,⁶⁵ M. L. Kocian,⁶⁵ D. W. G. S. Leith,⁶⁵ S. Li,⁶⁵ B. Lindquist,⁶⁵ S. Luitz,⁶⁵ V. Luth,⁶⁵ H. L. Lynch,⁶⁵ D. B. MacFarlane,⁶⁵ H. Marsiske,⁶⁵ R. Messner,^{65,*} D. R. Muller,⁶⁵ H. Neal,⁶⁵ S. Nelson,⁶⁵ C. P. O'Grady,⁶⁵ I. Ofte,⁶⁵ M. Perl,⁶⁵ B. N. Ratcliff,⁶⁵ A. Roodman,⁶⁵ A. A. Salnikov,⁶⁵ R. H. Schindler,⁶⁵ J. Schwiening,⁶⁵ A. Snyder,⁶⁵ D. Su,⁶⁵ M. K. Sullivan,⁶⁵ K. Suzuki,⁶⁵ S. K. Swain,⁶⁵ J. M. Thompson,⁶⁵ J. Va'vra,⁶⁵ A. P. Wagner,⁶⁵ M. Weaver,⁶⁵ C. A. West,⁶⁵ W. J. Wisniewski,⁶⁵ M. Wittgen,⁶⁵ D. H. Wright,⁶⁵ H. W. Wulsin,⁶⁵ A. K. Yarritu,⁶⁵ C. C. Young,⁶⁵ V. Ziegler,⁶⁵ X. R. Chen,⁶⁶ H. Liu,⁶⁶ W. Park,⁶⁶ M. V. Purohit,⁶⁶ R. M. White,⁶⁶ J. R. Wilson,⁶⁶ M. Bellis,⁶⁷ P. R. Burchat,⁶⁷ A. J. Edwards,⁶⁷ T. S. Miyashita,⁶⁷ S. Ahmed,⁶⁸ M. S. Alam,⁶⁸ J. A. Ernst,⁶⁸ B. Pan,⁶⁸ M. A. Saeed,⁶⁸ S. B. Zain,⁶⁸ A. Soffer,⁶⁹ S. M. Spanier,⁷⁰ B. J. Wogsland,⁷⁰ R. Eckmann,⁷¹ J. L. Ritchie,⁷¹ A. M. Ruland,⁷¹ C. J. Schilling,⁷¹ R. F. Schwitters,⁷¹ B. C. Wray,⁷¹ B. W. Drummond,⁷² J. M. Izen,⁷² X. C. Lou,⁷² F. Bianchi^{ab,73} D. Gamba^{ab,73} M. Pelliccioni^{ab,73} M. Bomben^{ab,74} L. Bosisio^{ab,74} C. Cartaro^{ab,74} G. Della Ricca^{ab,74} L. Lanceri^{ab,74} L. Vitale^{ab,74} V. Azzolini,⁷⁵ N. Lopez-March,⁷⁵ F. Martinez-Vidal,⁷⁵ D. A. Milanes,⁷⁵ A. Oyanguren,⁷⁵ J. Albert,⁷⁶ Sw. Banerjee,⁷⁶ B. Bhuyan,⁷⁶ H. H. F. Choi,⁷⁶ K. Hamano,⁷⁶ G. J. King,⁷⁶ R. Kowalewski,⁷⁶ M. J. Lewczuk,⁷⁶ I. M. Nugent,⁷⁶ J. M. Roney,⁷⁶ R. J. Sobie,⁷⁶ T. J. Gershon,⁷⁷ P. F. Harrison,⁷⁷ J. Ilic,⁷⁷ T. E. Latham,⁷⁷ G. B. Mohanty,⁷⁷ E. M. T. Puccio,⁷⁷ H. R. Band,⁷⁸ X. Chen,⁷⁸ S. Dasu,⁷⁸ K. T. Flood,⁷⁸ Y. Pan,⁷⁸ R. Prepost,⁷⁸ C. O. Vuosalo,⁷⁸ and S. L. Wu⁷⁸

(The BABAR Collaboration)

¹Laboratoire d'Annecy-le-Vieux de Physique des Particules (LAPP),
Université de Savoie, CNRS/IN2P3, F-74941 Annecy-Le-Vieux, France

²Universitat de Barcelona, Facultat de Física, Departament ECM, E-08028 Barcelona, Spain

³INFN Sezione di Bari^a; Dipartimento di Fisica, Università di Bari^b, I-70126 Bari, Italy

⁴University of Bergen, Institute of Physics, N-5007 Bergen, Norway

⁵Lawrence Berkeley National Laboratory and University of California, Berkeley, California 94720, USA

⁶University of Birmingham, Birmingham, B15 2TT, United Kingdom

⁷Ruhr Universität Bochum, Institut für Experimentalphysik 1, D-44780 Bochum, Germany

⁸University of British Columbia, Vancouver, British Columbia, Canada V6T 1Z1

⁹Brunel University, Uxbridge, Middlesex UB8 3PH, United Kingdom

¹⁰Budker Institute of Nuclear Physics, Novosibirsk 630090, Russia

¹¹University of California at Irvine, Irvine, California 92697, USA

¹²University of California at Riverside, Riverside, California 92521, USA

¹³University of California at San Diego, La Jolla, California 92093, USA

¹⁴University of California at Santa Barbara, Santa Barbara, California 93106, USA

¹⁵University of California at Santa Cruz, Institute for Particle Physics, Santa Cruz, California 95064, USA

¹⁶California Institute of Technology, Pasadena, California 91125, USA

¹⁷University of Cincinnati, Cincinnati, Ohio 45221, USA

¹⁸University of Colorado, Boulder, Colorado 80309, USA

¹⁹Colorado State University, Fort Collins, Colorado 80523, USA

²⁰Technische Universität Dortmund, Fakultät Physik, D-44221 Dortmund, Germany

²¹Technische Universität Dresden, Institut für Kern- und Teilchenphysik, D-01062 Dresden, Germany

²²Laboratoire Leprince-Ringuet, CNRS/IN2P3, Ecole Polytechnique, F-91128 Palaiseau, France

²³University of Edinburgh, Edinburgh EH9 3JZ, United Kingdom

²⁴INFN Sezione di Ferrara^a; Dipartimento di Fisica, Università di Ferrara^b, I-44100 Ferrara, Italy

²⁵INFN Laboratori Nazionali di Frascati, I-00044 Frascati, Italy

²⁶INFN Sezione di Genova^a; Dipartimento di Fisica, Università di Genova^b, I-16146 Genova, Italy

²⁷Harvard University, Cambridge, Massachusetts 02138, USA

²⁸Universität Heidelberg, Physikalisches Institut, Philosophenweg 12, D-69120 Heidelberg, Germany

²⁹Humboldt-Universität zu Berlin, Institut für Physik, Newtonstr. 15, D-12489 Berlin, Germany

³⁰Imperial College London, London, SW7 2AZ, United Kingdom

³¹University of Iowa, Iowa City, Iowa 52242, USA

³²Iowa State University, Ames, Iowa 50011-3160, USA

³³Johns Hopkins University, Baltimore, Maryland 21218, USA

³⁴Laboratoire de l'Accélérateur Linéaire, IN2P3/CNRS et Université Paris-Sud 11,
Centre Scientifique d'Orsay, B. P. 34, F-91898 Orsay Cedex, France

³⁵Lawrence Livermore National Laboratory, Livermore, California 94550, USA

³⁶University of Liverpool, Liverpool L69 7ZE, United Kingdom

³⁷Queen Mary, University of London, London, E1 4NS, United Kingdom

- ³⁸University of London, Royal Holloway and Bedford New College, Egham, Surrey TW20 0EX, United Kingdom
- ³⁹University of Louisville, Louisville, Kentucky 40292, USA
- ⁴⁰Johannes Gutenberg-Universität Mainz, Institut für Kernphysik, D-55099 Mainz, Germany
- ⁴¹University of Manchester, Manchester M13 9PL, United Kingdom
- ⁴²University of Maryland, College Park, Maryland 20742, USA
- ⁴³University of Massachusetts, Amherst, Massachusetts 01003, USA
- ⁴⁴Massachusetts Institute of Technology, Laboratory for Nuclear Science, Cambridge, Massachusetts 02139, USA
- ⁴⁵McGill University, Montréal, Québec, Canada H3A 2T8
- ⁴⁶INFN Sezione di Milano^a; Dipartimento di Fisica, Università di Milano^b, I-20133 Milano, Italy
- ⁴⁷University of Mississippi, University, Mississippi 38677, USA
- ⁴⁸Université de Montréal, Physique des Particules, Montréal, Québec, Canada H3C 3J7
- ⁴⁹Mount Holyoke College, South Hadley, Massachusetts 01075, USA
- ⁵⁰INFN Sezione di Napoli^a; Dipartimento di Scienze Fisiche, Università di Napoli Federico II^b, I-80126 Napoli, Italy
- ⁵¹NIKHEF, National Institute for Nuclear Physics and High Energy Physics, NL-1009 DB Amsterdam, The Netherlands
- ⁵²University of Notre Dame, Notre Dame, Indiana 46556, USA
- ⁵³Ohio State University, Columbus, Ohio 43210, USA
- ⁵⁴University of Oregon, Eugene, Oregon 97403, USA
- ⁵⁵INFN Sezione di Padova^a; Dipartimento di Fisica, Università di Padova^b, I-35131 Padova, Italy
- ⁵⁶Laboratoire de Physique Nucléaire et de Hautes Energies, IN2P3/CNRS, Université Pierre et Marie Curie-Paris6, Université Denis Diderot-Paris7, F-75252 Paris, France
- ⁵⁷University of Pennsylvania, Philadelphia, Pennsylvania 19104, USA
- ⁵⁸INFN Sezione di Perugia^a; Dipartimento di Fisica, Università di Perugia^b, I-06100 Perugia, Italy
- ⁵⁹INFN Sezione di Pisa^a; Dipartimento di Fisica, Università di Pisa^b; Scuola Normale Superiore di Pisa^c, I-56127 Pisa, Italy
- ⁶⁰Princeton University, Princeton, New Jersey 08544, USA
- ⁶¹INFN Sezione di Roma^a; Dipartimento di Fisica, Università di Roma La Sapienza^b, I-00185 Roma, Italy
- ⁶²Universität Rostock, D-18051 Rostock, Germany
- ⁶³Rutherford Appleton Laboratory, Chilton, Didcot, Oxon, OX11 0QX, United Kingdom
- ⁶⁴CEA, Irfu, SPP, Centre de Saclay, F-91191 Gif-sur-Yvette, France
- ⁶⁵SLAC National Accelerator Laboratory, Stanford, California 94309 USA
- ⁶⁶University of South Carolina, Columbia, South Carolina 29208, USA
- ⁶⁷Stanford University, Stanford, California 94305-4060, USA
- ⁶⁸State University of New York, Albany, New York 12222, USA
- ⁶⁹Tel Aviv University, School of Physics and Astronomy, Tel Aviv, 69978, Israel
- ⁷⁰University of Tennessee, Knoxville, Tennessee 37996, USA
- ⁷¹University of Texas at Austin, Austin, Texas 78712, USA
- ⁷²University of Texas at Dallas, Richardson, Texas 75083, USA
- ⁷³INFN Sezione di Torino^a; Dipartimento di Fisica Sperimentale, Università di Torino^b, I-10125 Torino, Italy
- ⁷⁴INFN Sezione di Trieste^a; Dipartimento di Fisica, Università di Trieste^b, I-34127 Trieste, Italy
- ⁷⁵IFIC, Universitat de Valencia-CSIC, E-46071 Valencia, Spain
- ⁷⁶University of Victoria, Victoria, British Columbia, Canada V8W 3P6
- ⁷⁷Department of Physics, University of Warwick, Coventry CV4 7AL, United Kingdom
- ⁷⁸University of Wisconsin, Madison, Wisconsin 53706, USA

We study the decay $B^- \rightarrow DK^{*-}$ using a sample of $379 \times 10^6 \Upsilon(4S) \rightarrow B\bar{B}$ events collected with the BABAR detector at the PEP-II B -factory. We perform a “GLW” analysis where the D meson decays into either a $CP+$ eigenstate ($K^+K^-, \pi^+\pi^-$), $CP-$ eigenstate ($K_S^0\pi^0, K_S^0\phi, K_S^0\omega$) or a non- CP state ($K^-\pi^+$). We also analyze D meson decays into $K^+\pi^-$ from a Cabibbo-favored \bar{D}^0 decay or doubly-suppressed D^0 decay (“ADS” analysis). We measure observables that are sensitive to the CKM angle γ : the partial-rate charge asymmetries $\mathcal{A}_{CP\pm}$, the ratios $\mathcal{R}_{CP\pm}$ of the B -decay branching fractions in $CP\pm$ and non- CP decay, the ratio \mathcal{R}_{ADS} of the charge-averaged branching fractions and the charge asymmetry \mathcal{A}_{ADS} of the ADS decays: $\mathcal{A}_{CP+} = 0.09 \pm 0.13 \pm 0.05$, $\mathcal{A}_{CP-} = -0.23 \pm 0.21 \pm 0.07$, $\mathcal{R}_{CP+} = 2.17 \pm 0.35 \pm 0.09$, $\mathcal{R}_{CP-} = 1.03 \pm 0.27 \pm 0.13$, $\mathcal{R}_{ADS} = 0.066 \pm 0.031 \pm 0.010$, $\mathcal{A}_{ADS} = -0.34 \pm 0.43 \pm 0.16$, where the first uncertainty is statistical and the second is systematic. Combining all the measurements and using a frequentist approach yields $r_B=0.24$ with a 68% confidence level interval of [0.18, 0.32] and exclude values of γ in the interval [55, 111] $^\circ$ at the 68% confidence level.

PACS numbers: 13.25.Hw, 14.40.Nd, 12.15.Hh, 11.30.Er

*Deceased

USA

†Now at Temple University, Philadelphia, Pennsylvania 19122,

I. INTRODUCTION

The Standard Model accommodates CP violation through a single phase in the Cabibbo-Kobayashi-Maskawa (CKM) quark mixing matrix V [1]. The self consistency of this mechanism can be tested by over-constraining the associated unitarity triangle [2, 3] using many different measurements, mostly involving decays of B mesons. In this paper we concentrate on the angle $\gamma = \arg(-V_{ud}V_{ub}^*/V_{cd}V_{cb}^*)$ by studying B meson decay channels where $b \rightarrow c\bar{u}s$ and $b \rightarrow u\bar{c}s$ tree amplitudes interfere. We use two techniques, one suggested by Gronau and London [4] and Gronau and Wyler [5] (GLW) and the other suggested by Atwood, Dunietz and Soni [6] (ADS) to study γ . Both techniques rely on final states that can be reached from both D^0 and \bar{D}^0 decays. As discussed in [7] the combination of the GLW and ADS observables can be very useful in resolving certain ambiguities inherent in each of the techniques.

In the GLW analysis the D meson [8] from $B^- \rightarrow DK^{*-}$ (892) [9] decays into either a $CP+$ eigenstate (K^+K^- , $\pi^+\pi^-$) or a $CP-$ eigenstate ($K_s\pi^0$, $K_s\phi$, $K_s\omega$). The size of the interference between the two competing amplitudes depends on the CKM angle γ as well as other parameters that are CP -conserving, discussed below. References [4, 5] define several observables that depend on measurable quantities:

$$\mathcal{R}_{CP\pm} = 2 \frac{\Gamma(B^- \rightarrow D_{CP\pm}^0 K^{*-}) + \Gamma(B^+ \rightarrow D_{CP\pm}^0 K^{*+})}{\Gamma(B^- \rightarrow D_{K\pi}^0 K^{*-}) + \Gamma(B^+ \rightarrow \bar{D}_{K\pi}^0 K^{*+})},$$

$$\mathcal{A}_{CP\pm} = \frac{\Gamma(B^- \rightarrow D_{CP\pm}^0 K^{*-}) - \Gamma(B^+ \rightarrow D_{CP\pm}^0 K^{*+})}{\Gamma(B^- \rightarrow D_{CP\pm}^0 K^{*-}) + \Gamma(B^+ \rightarrow D_{CP\pm}^0 K^{*+})}.$$

Here $D_{CP\pm}^0$ refers to a neutral D meson decaying into either a $CP+$ or $CP-$ eigenstate.

$\mathcal{R}_{CP\pm}$ and $\mathcal{A}_{CP\pm}$ depend on the physical parameters as follows:

$$\mathcal{R}_{CP\pm} = 1 + r_B^2 \pm 2r_B \cos \delta_B \cos \gamma, \quad (1)$$

$$\mathcal{A}_{CP\pm} = \pm 2r_B \sin \delta_B \sin \gamma / \mathcal{R}_{CP\pm}. \quad (2)$$

Here r_B is the magnitude of the ratio of the suppressed and favored amplitudes $B^- \rightarrow \bar{D}^0 K^{*-}$ and $B^- \rightarrow D^0 K^{*-}$ decays, respectively, and δ_B is the CP -conserving phase difference between these amplitudes. In this analysis we neglect the effects of CP violation in D meson decays, as justified in Ref. [10], due to the very small effect of $D^0\bar{D}^0$ mixing.

We define two additional quantities whose experimental estimators are normally distributed even when the value of r_B is comparable to its uncertainty:

$$x_{\pm} = r_B \cos(\gamma \pm \delta_B) \quad (3)$$

$$= \frac{R_{CP+}(1 \mp \mathcal{A}_{CP+}) - R_{CP-}(1 \mp \mathcal{A}_{CP-})}{4}.$$

Since x_{\pm} are also directly measured in Dalitz-plot analyses [11], the different results can be compared and combined with each other. We note that an additional set

of quantities measured in Dalitz-plot analyses, $y_{\pm} = r_B \sin(\gamma \pm \delta_B)$, are not accessible through the GLW analysis.

In the ADS technique, $B^- \rightarrow DK^{*-}$ can decay into $[K^+\pi^-]_D K^{*-}$ where $[K^+\pi^-]_D$ indicates that these particles are neutral D meson (D^0 or \bar{D}^0) decay products. This final state can be reached from the doubly-Cabibbo-suppressed decay $D^0 \rightarrow K^+\pi^-$ or $B^- \rightarrow \bar{D}^0 K^{*-}$ followed by the Cabibbo-favored decay $\bar{D}^0 \rightarrow K^+\pi^-$. In addition, the final state $[K^-\pi^+]_D K^{*-}$ is used for normalization. We label the decays where the K and K^* have the same (opposite) charge as “right (wrong) sign” where the labels reflect that one mode occurs much more often than the other.

In analogy with the GLW method we define two measurable quantities, \mathcal{R}_{ADS} and \mathcal{A}_{ADS} , as follows:

$$\mathcal{R}_{ADS} = \frac{\Gamma(B^- \rightarrow [K^+\pi^-]_D K^{*-}) + \Gamma(B^+ \rightarrow [K^-\pi^+]_D K^{*+})}{\Gamma(B^- \rightarrow [K^-\pi^+]_D K^{*-}) + \Gamma(B^+ \rightarrow [K^+\pi^-]_D K^{*+})},$$

$$\mathcal{A}_{ADS} = \frac{\Gamma(B^- \rightarrow [K^+\pi^-]_D K^{*-}) - \Gamma(B^+ \rightarrow [K^-\pi^+]_D K^{*+})}{\Gamma(B^- \rightarrow [K^+\pi^-]_D K^{*-}) + \Gamma(B^+ \rightarrow [K^-\pi^+]_D K^{*+})}.$$

\mathcal{R}_{ADS} and \mathcal{A}_{ADS} are related to physically interesting quantities by:

$$\mathcal{R}_{ADS} = r_D^2 + r_B^2 + 2r_D r_B \cos(\delta_B + \delta_D) \cos \gamma, \quad (4)$$

$$\mathcal{A}_{ADS} = 2r_D r_B \sin(\delta_B + \delta_D) \sin \gamma / \mathcal{R}_{ADS}. \quad (5)$$

Here r_D is the magnitude of the ratio of suppressed and favored amplitudes of the decays $D^0 \rightarrow K^+\pi^-$ and $D^0 \rightarrow K^-\pi^+$ decays, respectively, while δ_D is the CP -conserving strong phase difference between these two amplitudes. Both r_D and δ_D have been measured and we use the values given in [12]: $r_D = 0.0578 \pm 0.0008$ and $\delta_D = 22.5_{-11.0}^{+10.4}$. Estimates for r_B are in the range $0.1 \leq r_B \leq 0.3$ [13, 14].

It has been pointed out in Ref. [13] that complications due to possible variations in r_B and/or δ_B as a result of the finite width of a resonance such as the K^* and its overlap with other states can be taken into account using an alternate formalism. However, in this paper we choose to follow the procedures in [14, 15] and incorporate the effects of the non- $K^* DK\pi$ events and finite width of the K^* into the systematic uncertainties of our \mathcal{A} 's and \mathcal{R} 's.

II. THE BABAR DETECTOR AND DATASET

The *BABAR* detector has been described in detail in [16] and therefore will only be briefly discussed here. The trajectories of charged tracks are measured with a five-layer double-sided silicon vertex tracker (SVT) and a 40-layer drift chamber (DCH). Both the SVT and DCH are located inside a 1.5-T solenoidal magnetic field. Photons are detected by means of a CsI(Tl) crystal calorimeter also located inside the magnet. Charged particle identification is determined from information provided by a ring-imaging Cherenkov device (DIRC) in combination

[‡]Also with Università di Perugia, Dipartimento di Fisica, Perugia, Italy

[§]Also with Università di Roma La Sapienza, I-00185 Roma, Italy

with ionization measurements (dE/dx) from the tracking detectors. The *BABAR* detector's response to various physics processes as well as varying beam and environmental conditions is modeled with simulation software based on the GEANT4 [17] toolkit. We use EVTGEN [18] to model the kinematics of B mesons and JETSET [19] to model continuum processes ($e^+e^- \rightarrow c\bar{c}, u\bar{u}, d\bar{d}, s\bar{s}$). This analysis uses data collected at and near the $\Upsilon(4S)$ resonance with the *BABAR* detector at the PEP-II storage ring. The data set consists of 345 fb^{-1} collected at the peak of the $\Upsilon(4S)$ ($379 \times 10^6 B\bar{B}$ pairs) and 35 fb^{-1} 40 MeV below the resonance peak (off-peak data).

This analysis is a combined update of the previous *BABAR* GLW [15] and ADS [14] studies of $B^- \rightarrow D^0 K^{*-}$ which used $232 \times 10^6 B\bar{B}$ pairs. Other new features in this analysis include improvement in background suppression, refinement of various candidate selection criteria, and update of systematic uncertainties. The major change is the choice of neural networks in the GLW analysis over Fisher discriminants, which were used in the previous analysis. We verify the improvements on both signal efficiency and continuum background rejection in the GLW decay channels with simulated signal and continuum events. The increases in signal efficiency range from 3% to 14% for all channels except $K_s^0\phi$, which has the same efficiency. For continuum suppression, the neural networks perform 10% to 57% better across all channels except K^+K^- , which displays the same performance.

III. THE GLW ANALYSIS

We reconstruct $B^- \rightarrow DK^{*-}$ with the subsequent decays $K^{*-} \rightarrow K_s^0\pi^-$, $K_s^0 \rightarrow \pi^+\pi^-$ and with the D decaying into six decay final states, $D^0 \rightarrow K^-\pi^+$ (non- CP final state); K^+K^- , $\pi^+\pi^-$ ($CP+$ eigenstates); and $K_s^0\pi^0$, $K_s^0\phi$, $K_s^0\omega$ ($CP-$ eigenstates). We optimize our event selection criteria by maximizing the figure of merit $S/\sqrt{S+B}$, with S the number of signal events and B the number of background events, determined for each channel using simulated signal and background events. Kaon and pion candidates (except for the pions from K_s^0 decays) are selected using a likelihood-based particle identification algorithm which relies on dE/dx information measured in the DCH and the SVT, and Cherenkov photons in the DIRC. The efficiency of the selectors are typically above 85% for momenta below 4 GeV while the kaon and pion fake rate is at the few percent level for particles in this momentum range.

The K_s^0 candidates are formed from oppositely charged tracks assumed to be pions with a reconstructed invariant mass within 13 MeV/ c^2 (four standard deviations) of the known K_s^0 mass [3], $m_{K_s^0}$. All K_s^0 candidates are refitted so that their invariant mass equals $m_{K_s^0}$ (mass constraint). They are also constrained to emerge from a single vertex (vertex constraint). For those retained to build a K^{*-} candidate we further require that their

flight direction and length be consistent with a K_s^0 coming from the interaction point. The K_s^0 candidate flight path and momentum must make an acute angle and the flight length in the plane transverse to the beam direction must exceed its uncertainty by three standard deviations. K^{*-} candidates are formed from a K_s^0 and a charged particle with a vertex constraint. We select K^{*-} candidates which have an invariant mass within 75 MeV/ c^2 of the known mean value for a K^* [3]. Finally, since the K^{*-} in $B^- \rightarrow DK^{*-}$ is longitudinally polarized, we require $|\cos\theta_H| \geq 0.35$, where θ_H is the angle in the K^{*-} rest frame between the daughter pion momentum and the parent B momentum. The helicity distribution discriminates well between a B meson decay and a false B meson candidate from the continuum, since the former is distributed as $\cos^2\theta_H$ and the latter has a flat distribution.

Some decay modes of the D contain a π^0 . We combine pairs of photons to form a π^0 candidate with a total energy greater than 200 MeV and an invariant mass between 115 and 150 MeV/ c^2 . A mass constrained fit is applied to the selected π^0 candidate momenta. Composite particles (ϕ and ω) included in the $CP-$ modes are vertex-constrained. Candidate ϕ (ω) mesons are constructed from K^+K^- ($\pi^+\pi^-\pi^0$) particle combinations with the invariant mass required to be within 12 (20) MeV/ c^2 or two standard deviations of the known peak values [3]. Two further requirements are made on the ω candidates. The magnitude of the cosine of the helicity angle between the D momentum in the rest frame of the ω and the normal to the plane containing all three decay pions must be greater than 0.35 (it has a $\cos^2\theta_H$ distribution for signal candidates and is flat for background). The Dalitz angle [20], θ_D , is defined as the angle between the momentum of one daughter pion in the ω rest frame and the direction of one of the other two pions in the rest frame of the two pions. For signal candidates, the cosine of the Dalitz angle follows a $\sin^2\theta_D$ distribution; while it is flat for the background. Therefore we require the cosine of the Dalitz angle of signal candidates to have a magnitude smaller than 0.8.

Except for the $K_s^0\pi^0$ final state, all D candidates are mass and vertex constrained. We select D candidates with an invariant mass differing from the known mass [3] by less than 12 MeV/ c^2 for all channels except $K_s^0\pi^0$ (30 MeV/ c^2) and $K_s^0\omega$ (20 MeV/ c^2). These limits are about twice the corresponding RMS mass resolutions.

Suppression of backgrounds from continuum events is achieved by using event-shape and angular variables. The B meson candidate is required to have $|\cos\theta_T| \leq 0.9$, where θ_T is the angle between the thrust axis of the B meson and that of the rest of the event. The distribution of $|\cos\theta_T|$ is uniform in $B\bar{B}$ events and strongly peaked near 1 for continuum events.

A neural network (NN) is used to further reduce the $q\bar{q}$ ($q = u, d, s, c$) contribution to our data sample. Seven variables are used in the NN with three being the angular moments L_0 , L_1 and L_2 . These moments are de-

202 fined by: $L_j = \sum_i p_i^* |\cos \theta_i^*|^j$ where the sum is over
 203 charged and neutral particles not associated with the
 204 B meson candidate. Here p_i^* ($\cos \theta_i^*$) is the momen-
 205 tum (angle) of the i th particle with respect to the thrust
 206 of the candidate B meson in the center-of-mass (CM)
 207 frame. Additional details on the moments can be found
 208 in Ref. [21]. The NN also uses the ratio $R_2 = H_2/H_0$ of
 209 Fox-Wolfram moments [22], the cosine of the angle be-
 210 tween the B candidate momentum vector and the beam
 211 axis ($\cos \theta_B$), $\cos \theta_T$ (defined above), and the cosine of
 212 the angle between a D^0 daughter momentum vector in
 213 the D^0 rest frame and the direction of the D^0 in the
 214 B meson rest frame ($\cos \theta_H(D^0)$). The distributions of
 215 all the above variables show distinct differences between
 216 signal and continuum events and thus can be exploited
 217 by a NN to select out $B\bar{B}$ events. Each decay mode
 218 has its own unique NN trained with signal and contin-
 219 uum Monte Carlo events. After training, the NNs are
 220 then fed with independent sets of signal and continuum
 221 Monte Carlo events to produce NN outputs for various
 222 decay modes. Finally, we verify that the NNs have con-
 223 sistent outputs for off-peak data (continuum data col-
 224 lected below the $\Upsilon(4S)$) and $q\bar{q}$ Monte Carlo events. The
 225 separations between signal and continuum background
 226 are shown in Fig. 1. We select candidates with neural
 227 network output above 0.65 (K^+K^-), 0.82 ($\pi^+\pi^-$), 0.91
 228 ($K_S^0\pi^0$), 0.56 ($K_S^0\phi$), 0.80 ($K_S^0\omega$), and 0.73 ($K^-\pi^+$). Our
 229 event selection is optimized to maximize the significance
 230 of the signal yield, determined using simulated signal and
 231 background events.

232 We identify B candidates using two nearly independ-
 233 ent kinematic variables: the beam-energy-substituted
 234 mass $m_{ES} = \sqrt{(s/2 + \mathbf{p}_0 \cdot \mathbf{p}_B)^2/E_0^2 - p_B^2}$ and the energy
 235 difference $\Delta E = E_B^* - \sqrt{s}/2$, where E and p are energy
 236 and momentum. The subscripts 0 and B refer to the
 237 e^+e^- -beam system and the B candidate, respectively; s
 238 is the square of the CM energy and the asterisk labels
 239 the CM frame. The m_{ES} distributions are all described
 240 by a Gaussian function \mathcal{G} centered at the B mass with
 241 a resolution of 2.50, 2.55 and 2.51 MeV/ c^2 for the $CP+$,
 242 $CP-$ and non- CP mode, respectively. The ΔE distri-
 243 butions are centered on zero for signal with a resolution
 244 of 11 to 13 MeV for all channels except $K_S^0\pi^0$ for which
 245 the resolution is asymmetric and is about 30 MeV. We
 246 define a signal region through the requirement $|\Delta E| <$
 247 50 (25) MeV for $K_S^0\pi^0$ (all other modes).

248 A potentially dangerous background for $B^- \rightarrow$
 249 $D(\pi^+\pi^-)K^{*-}(K_S^0\pi^-)$ is the decay mode $B^- \rightarrow$
 250 $D(K_S^0\pi^+\pi^-)\pi^-$ which contains the same final-state par-
 251 ticles as the signal but has a branching fraction 600
 252 times larger. We therefore explicitly veto any selected
 253 B candidate containing a $K_S^0\pi^+\pi^-$ combination within
 254 60 MeV/ c^2 of the D^0 mass.

255 The fraction of events with more than one acceptable
 256 B candidate depends on the D decay mode and is always
 257 less than 7.8%. To select the best B candidate in those
 258 events where we find more than one acceptable candidate,
 259 we choose the one with the smallest χ^2 formed from the

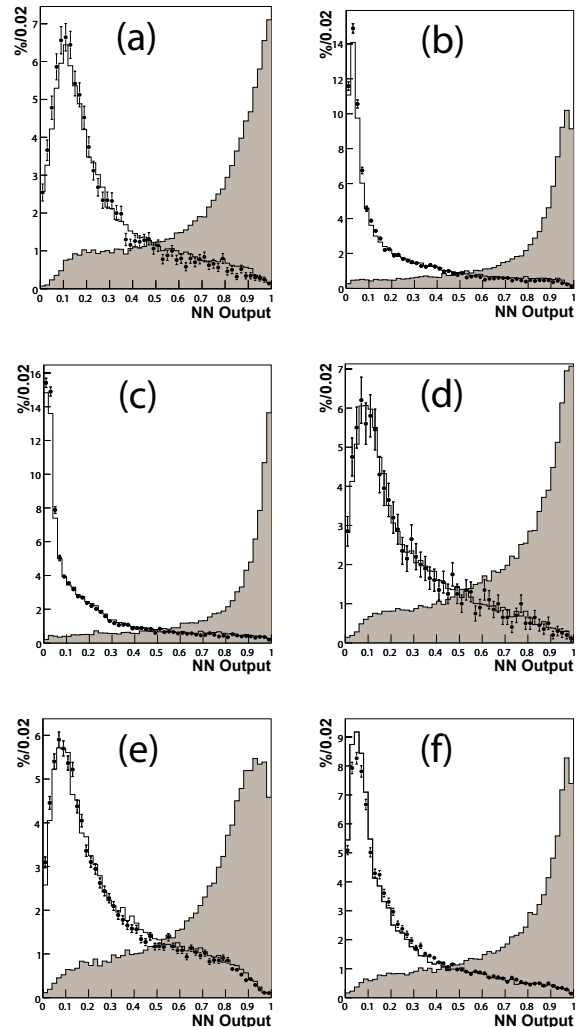


FIG. 1: The neural network (NN) outputs and results of the NN verifications of (a) K^+K^- , (b) $\pi^+\pi^-$, (c) $K_S^0\pi^0$, (d) $K_S^0\phi$, (e) $K_S^0\omega$, and (f) $K^-\pi^+$ subsamples of the GLW analysis. The samples used to produce the output are shown as histograms. The signal (Monte Carlo simulation) is the shaded histogram peaking near 1; the continuum (Monte Carlo simulation) is the histogram peaking near 0. The off-peak data used to check the NN are overlaid as data points.

260 differences of the measured and true D^0 and K^{*-} masses
 261 divided by the mass spread which includes the resolution
 262 and, for the K^{*-} , the natural width:

$$\begin{aligned} \chi^2 &= \chi_{M_{D^0}}^2 + \chi_{M_{K^{*-}}}^2 \quad (6) \\ &= \frac{(M_{D^0} - M_{D^0}^{PDG})^2}{\sigma_{M_{D^0}}^2} + \frac{(M_{K^{*-}} - M_{K^{*-}}^{PDG})^2}{\sigma_{M_{K^{*-}}}^2 + \Gamma_{K^{*-}}^2/c^4}. \end{aligned}$$

263 Simulations show that no bias is introduced by this choice
 264 and the correct candidate is picked at least 86% of the
 265 time.

266 According to simulation of signal events, the total re-

267 construction efficiencies are: 12.8% and 12.3% for the
 268 $CP+$ modes $D \rightarrow K^+K^-$ and $\pi^+\pi^-$; 5.6%, 8.9%, and
 269 2.4% for the $CP-$ modes $D \rightarrow K_s^0\pi^0$, $K_s^0\phi$ and $K_s^0\omega$;
 270 12.8% for the non- CP mode $D^0 \rightarrow K^-\pi^+$.

271 To study $B\bar{B}$ backgrounds we look in sideband regions
 272 in ΔE and m_{D^0} . We define the ΔE sideband in the
 273 interval $60 \leq \Delta E \leq 200$ MeV for all modes. This region is
 274 used to determine the combinatorial background shapes
 275 in the signal and m_D sideband. We choose not to use a
 276 lower sideband because of the D^*K^* backgrounds in that
 277 region. The sideband region in m_D is defined by requiring
 278 that m_D differs from the D^0 mass by more than four
 279 standard deviations. This region provides sensitivity to
 280 background sources which mimic signal both in ΔE and
 281 m_{ES} and originates from either charmed or charmless B
 282 meson decays that do not contain a true D . As many of
 283 the possible contributions to this background are not well
 284 known, we measure its size by including the m_D sideband
 285 in the fit described below.

286 An unbinned extended maximum likelihood fit to the
 287 m_{ES} distributions of selected B candidates in the range
 288 $5.2 \leq m_{ES} \leq 5.3$ GeV/c^2 is used to determine signal
 289 and background yields and the CP -violating quantities
 290 \mathcal{A}_{CP} and \mathcal{R}_{CP} . We use the same mean and width of the
 291 Gaussian function \mathcal{G} to describe the signal shape for all
 292 modes considered. The combinatorial background in the
 293 m_{ES} distribution is modeled with the so called ‘‘ARGUS’’
 294 empirical threshold function \mathcal{A} [23]. It is defined as:

$$\mathcal{A}(m_{ES}) \propto m_{ES} \sqrt{1 - x^2} \exp^{-\xi(1-x^2)}, \quad (7)$$

295 where $x = m_{ES}/E_{\text{max}}$ and E_{max} is the maximum mass for
 296 pair-produced B mesons given the collider beam energies
 297 and is fixed in the fit at 5.291 GeV/c^2 . The ARGUS
 298 shape is governed by one parameter ξ that is left free in
 299 the fit. We fit simultaneously m_{ES} distributions of nine
 300 samples: the non- CP , $CP+$ and $CP-$ samples for (i)
 301 the signal region, (ii) the m_D sideband and (iii) the ΔE
 302 sideband. In addition the signal region is divided into two
 303 samples according to the charge of the B candidate. We
 304 fit three probability density functions (PDF) weighted by
 305 the unknown event yields. For the ΔE sideband, we use
 306 \mathcal{A} . For the m_D sideband (sb) we use $a_{sb} \cdot \mathcal{A} + b_{sb} \cdot \mathcal{G}$,
 307 where \mathcal{G} accounts for fake- D candidates. For the signal
 308 region PDF, we use $a \cdot \mathcal{A} + b \cdot \mathcal{G}_{\text{peak}} + c \cdot \mathcal{G}_{\text{signal}}$, where b
 309 is scaled from b_{sb} with the assumption that the number of
 310 fake D background present in the signal region is equal to
 311 the number measured in the m_D sideband scaled by the
 312 ratio of the m_D signal-window to sideband widths, and c
 313 is the number of $B^\pm \rightarrow D^0 K^{*\pm}$ signal events. The non-
 314 CP mode sample, with relatively high statistics, helps
 315 constrain the PDF shapes for the low statistics CP mode
 316 distributions. The ΔE sideband sample helps determine
 317 the \mathcal{A} background shape. In total, the fit determines 19
 318 event yields as well as the mean and width of the signal
 319 Gaussian and the ARGUS parameter ξ .

320 Since the values of ξ obtained for each data sample
 321 are consistent with each other, albeit with large statisti-
 322 cal uncertainties, we have constrained ξ to have the

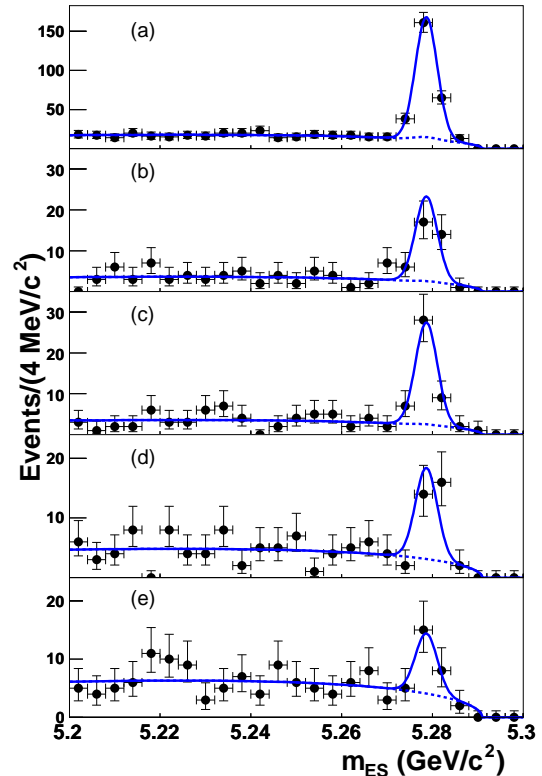


FIG. 2: Distributions of m_{ES} in the signal region for (a) the non- CP modes in B^\pm decays, (b) the $CP+$ modes in B^+ and (c) B^- decays and (d) the $CP-$ modes in B^+ and (e) B^- decays. The dashed curve indicates the total background contribution which includes the fake D background estimated from a simultaneous fit to the m_D sideband.

323 same value for all data samples in the fit. The simulation
 324 shows that the use of the same Gaussian parameters
 325 for all signal modes introduces only negligible systemat-
 326 ic corrections. We assume that the fake D background
 327 found in the m_D sideband have the same final states as
 328 the signal and we fit it with the same Gaussian.

329 The fake D background is assumed to not violate CP
 330 and is therefore split equally between the B^- and B^+
 331 sub-samples. This assumption is consistent with results
 332 from our simulations and is considered further when we
 333 discuss the systematic uncertainties. The fit results are
 334 shown graphically in Fig. 2 and numerically in Table I.
 335 Table II records the number of events measured for each
 336 individual D decay mode.

337 Although most systematic uncertainties cancel for
 338 \mathcal{A}_{CP} , an asymmetry inherent to the detector or data
 339 processing may exist. We quote the results from the
 340 study carried out in [24], where we used $B^- \rightarrow D^0\pi^-$
 341 (with D^0 decays into CP or non- CP eigenstates) events
 342 from control samples of data and simulation to measure
 343 the charge asymmetry. An average charge asymmetry of
 344 $A_{ch} = (-1.6 \pm 0.6)\%$ was measured. We add linearly
 345 the central value and one-standard deviation in the most

TABLE I: Results from the fit. For each GLW D mode, we give the number of measured signal events, the fake D contribution, \mathcal{A}_{CP} and \mathcal{R}_{CP} . The fake D contribution is calculated by scaling the the number of fake D events found in the m_D sideband region to the signal region. The uncertainties are statistical only. We also show the number of measured signal events split by the B charge for $CP+$ and $CP-$ modes.

	# Signal	# Fake D	\mathcal{A}_{CP}	\mathcal{R}_{CP}
Non- CP	231 ± 17	5.0		
$CP+$	68.6 ± 9.2	0.3	0.09 ± 0.13	2.17 ± 0.35
(B^+)	31.2 ± 6.2			
(B^-)	37.4 ± 6.8			
$CP-$	38.5 ± 7.0	0.0	-0.23 ± 0.21	1.03 ± 0.27
(B^+)	23.0 ± 4.8			
(B^-)	15.5 ± 5.2			

TABLE II: Number of signal events from the GLW fit for individual D decay modes studied in this analysis. We also provide the selection efficiencies (in %). The uncertainties are statistical only.

	# Signal	Selection Efficiency (%)
Non- CP		
$K^- \pi^+$	231 ± 17	12.76 ± 0.09
$CP+$		
$K^+ K^-$	41 ± 7	12.78 ± 0.05
$\pi^+ \pi^-$	28 ± 6	12.34 ± 0.05
$CP-$		
$K_S^0 \pi^0$	21 ± 7	5.59 ± 0.03
$K_S^0 \phi$	8 ± 3	8.90 ± 0.04
$K_S^0 \omega$	9 ± 4	2.35 ± 0.02

conservative direction to assign a systematic uncertainty of 2.2%. The second substantial systematic effect is a possible CP asymmetry in the fake D background which cannot be excluded due to CP violation in charmless B decays. If there is an asymmetry $\mathcal{A}_{\text{fake } D}$, then the systematic uncertainty on \mathcal{A}_{CP} is $\mathcal{A}_{\text{fake } D} \times \frac{b}{c}$, where b is the contribution of the fake D background and c the signal yield. Assuming conservatively $|\mathcal{A}_{\text{fake } D}| \leq 0.5$, we obtain systematic uncertainties of ± 0.003 and ± 0.040 on \mathcal{A}_{CP+} and \mathcal{A}_{CP-} respectively. Note that since we do not observe any fake D background in $CP-$ modes, we use the statistical uncertainty of the signal yield from the fit to estimate this systematic uncertainty.

Since \mathcal{R}_{CP} is a ratio of rates of processes with different final states of the D , we must consider the uncertainties affecting the selection algorithms for the different D channels. This results in small correction factors which account for the difference between the actual detector response and the simulation model. The main effects stem from the approximate modeling of the tracking efficiency (a correction of 0.4% per pion track coming from a K_S^0 and 0.2% per kaon and pion track coming from other candidates), the K_S^0 reconstruction efficiency for $CP-$ modes of the D^0 (1.3% per K_S^0 in $K_S^0 \phi$ mode and 2.0%

in $K_S^0 \pi^0$ and $K_S^0 \omega$), the π^0 reconstruction efficiency for the $K_S^0 \pi^0$ and $K_S^0 [\pi^+ \pi^- \pi^0]_\omega$ channels (3%) and the efficiency and misidentification probabilities from the particle identification (2% per track). The correction factors are calculated by comparing data and Monte Carlo using high-statistics and high-purity samples. Charged kaon and pion samples obtained from D meson decays ($D^{*+} \rightarrow D^0 \pi^+$) are used for particle identification corrections. For tracking corrections, we use τ -pair events where one τ decays to a muon and two neutrinos and the other decays to $\rho^0 h \nu$ where h is a K or a π . $B^0 \rightarrow \phi K_S^0$ and $B^0 \rightarrow \pi^+ D^-$ ($D^- \rightarrow K_S^0 \pi^-$) decays are used for K_S^0 corrections, and π^0 correction factors are calculated using $\tau \rightarrow \rho \nu$ and $\tau \rightarrow \pi \nu$ samples. Altogether, the systematic uncertainties due to total efficiency corrections equal ± 0.078 and ± 0.100 for \mathcal{R}_{CP+} and \mathcal{R}_{CP-} , respectively. The uncertainty on the measured branching fractions for different D decay modes [3], is included in the calculation of the efficiency corrections.

Another systematic correction applied to the $CP-$ measurements arises from a possible $CP+$ background in the $K_S^0 \phi$ and $K_S^0 \omega$ channels. In this case, the observed quantities $\mathcal{A}_{CP-}^{\text{obs}}$ and $\mathcal{R}_{CP-}^{\text{obs}}$ are corrected:

$$\mathcal{A}_{CP-} = (1 + \epsilon) \mathcal{A}_{CP-}^{\text{obs}} - \epsilon \mathcal{A}_{CP+}; \quad \mathcal{R}_{CP-} = \frac{\mathcal{R}_{CP-}^{\text{obs}}}{(1 + \epsilon)},$$

where ϵ is the ratio of $CP+$ background to $CP-$ signal. An investigation of the $D^0 \rightarrow K^- K^+ K_S^0$ Dalitz plot [25] indicates that the dominant background for $D^0 \rightarrow K_S^0 \phi$ comes from the decay $a_0(980) \rightarrow K^+ K^-$, at the level of $(25 \pm 1)\%$ of the size of the ϕK_S^0 signal. We have no information for the ωK_S^0 channel and assume $(30 \pm 30)\%$ of $CP+$ background contamination. The $K_S^0 \pi^0$ mode has no $CP+$ background. The value of ϵ for the combination of $CP-$ modes is $(11 \pm 7)\%$. The systematic uncertainty associated with this effect is ± 0.02 and ± 0.06 for \mathcal{A}_{CP-} and \mathcal{R}_{CP-} , respectively.

To account for the non resonant $K_S^0 \pi^-$ pairs in the K^* mass range we study a model that incorporates S -wave and P -wave pairs in both the $b \rightarrow c \bar{u} s$ and $b \rightarrow u \bar{c} s$ amplitudes. The P -wave mass dependence is described by a single relativistic Breit-Wigner while the S -wave component is assumed to be a complex constant. It is expected that higher order partial waves will not contribute significantly and therefore they are neglected in the model. We also assume that the same amount of S and P -wave is present in the $b \rightarrow c \bar{u} s$ and $b \rightarrow u \bar{c} s$ amplitudes. The amount of S -wave present in the favored $b \rightarrow c \bar{u} s$ amplitude is determined directly from the data by fitting the angular distribution of the $K_S^0 \pi$ system in the K^* mass region, accounting for interference [26]. From this fit we determine that the number of non- $K^* K_S^- \pi^-$ events is $(4 \pm 1)\%$ of the measured signal events. To estimate the systematic uncertainties due to this source we vary all the strong phases between 0 and 2π and calculate the maximum deviation between the S -wave model and the expectation if there were no non-resonant contribution for both $\mathcal{A}_{CP\pm}$ (Eq. (2)) and $\mathcal{R}_{CP\pm}$ (Eq. (1)). This

background induces systematic variations of ± 0.051 for $\mathcal{A}_{CP\pm}$ and ± 0.035 for $\mathcal{R}_{CP\pm}$.

The last systematic uncertainty is due to the assumption that the parameters of the Gaussian and ARGUS functions are the same throughout signal region, ΔE and m_{D^0} sidebands. We estimate the uncertainties by varying the width and mean of the Gaussian and ξ of the ARGUS by their corresponding statistical uncertainties obtained from the fit. All the systematic uncertainties are listed in Table III. We add them in quadrature and quote the final results:

$$\begin{aligned}\mathcal{A}_{CP+} &= 0.09 \pm 0.13(\text{stat.}) \pm 0.05(\text{syst.}) \\ \mathcal{A}_{CP-} &= -0.23 \pm 0.21(\text{stat.}) \pm 0.07(\text{syst.}) \\ \mathcal{R}_{CP+} &= 2.17 \pm 0.35(\text{stat.}) \pm 0.09(\text{syst.}) \\ \mathcal{R}_{CP-} &= 1.03 \pm 0.27(\text{stat.}) \pm 0.13(\text{syst.})\end{aligned}$$

TABLE III: Summary of systematic uncertainties for the GLW analysis.

Source	$\delta\mathcal{A}_{CP+}$	$\delta\mathcal{A}_{CP-}$	$\delta\mathcal{R}_{CP+}$	$\delta\mathcal{R}_{CP-}$
Detection asymmetry	0.002	0.004	-	-
Non-resonant $K_s^0\pi^-$ bkg.	0.051	0.051	0.035	0.035
Same-final-state bkg.	-	0.019	-	0.061
Asymmetry in fake D^0 bkg.	0.003	0.040	-	-
Efficiency correction	-	-	0.078	0.100
Same \mathcal{G} and \mathcal{A} shape	0.003	0.013	0.009	0.025
Total systematic uncertainty	0.051	0.069	0.086	0.125

These results can also be expressed in terms of x_{\pm} defined in Eq. (3) :

$$\begin{aligned}x_+ &= 0.21 \pm 0.14 (\text{stat.}) \pm 0.05 (\text{syst.}), \\ x_- &= 0.40 \pm 0.14 (\text{stat.}) \pm 0.05 (\text{syst.}),\end{aligned}$$

where the $CP+$ pollution systematic effects are included. Including these effects increased x_+ and x_- by 0.035 ± 0.024 and 0.023 ± 0.017 , respectively.

IV. THE ADS ANALYSIS

In the ADS analysis we only use D decays with a charged kaon and pion in the final state and K^{*-} decays to $K_s^0\pi^-$ followed by $K_s^0 \rightarrow \pi^+\pi^-$. The ADS event selection criteria and procedures are nearly identical to those used for the GLW analysis. However due to the small value of r_D the yield of interesting ADS events (i.e. $B^- \rightarrow [K^+\pi^-]_D K^{*-}$ and $B^+ \rightarrow [K^-\pi^+]_D K^{*+}$) is expected to be smaller than for the GLW analysis. Therefore in order to reduce the background in the ADS analysis the K_s^0 invariant mass window is narrowed to $10 \text{ MeV}/c^2$ and the K^{*-} invariant mass cut is reduced to $55 \text{ MeV}/c^2$. A neural network using the same variables as in the GLW analysis is trained on ADS signal and

continuum MC events and verified using off-peak continuum data. The separation between signal and continuum background is shown in Fig. 3. We select candidates with neural network output above 0.85. All other K_s^0 , K^{*-} , and continuum suppression criteria are the same as those used in the GLW analysis.

$D \rightarrow K^-\pi^+$ and $K^+\pi^-$ candidates are used in this analysis. Candidates that have an invariant mass within $18 \text{ MeV}/c^2$ (2.5 standard deviations) of the nominal D^0 mass [3] are kept for further study. We require kaon candidates to pass the same particle identification criteria as imposed in the GLW analysis.

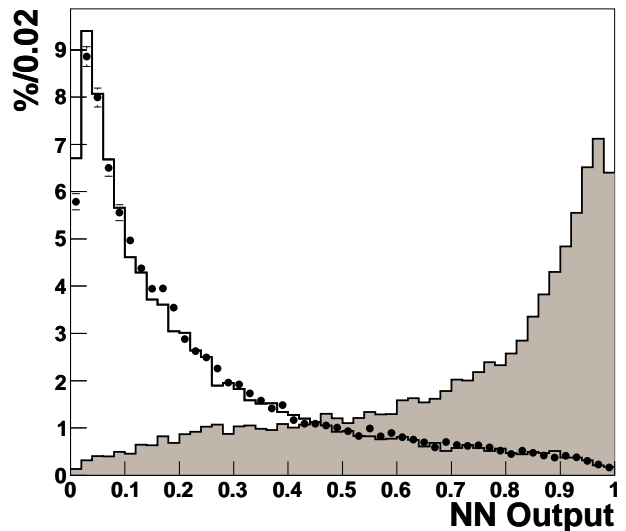


FIG. 3: The neural network (NN) output and result of the NN verification for the ADS analysis (see text). The samples used to produce the output are shown as histograms. The signal (Monte Carlo simulation) is the shaded histogram peaking near 1; the continuum (Monte Carlo simulation) is the histogram peaking near 0. The off-peak data used to check the NN are overlaid as data points.

We identify B meson candidates using the beam-energy-substituted mass m_{ES} and the energy difference ΔE . For this analysis signal candidates must satisfy $|\Delta E| \leq 25 \text{ MeV}$. The efficiency to detect a $B^- \rightarrow D^0 K^{*-}$ signal event where $D^0 \rightarrow K\pi$, after all criteria are imposed, is $(9.6 \pm 0.1)\%$. This efficiency is the same for $D^0 \rightarrow K^-\pi^+$ and $D^0 \rightarrow K^+\pi^-$. In 1.8% of the events we find more than one suitable candidate. In such cases we choose the candidate with the smallest χ^2 defined in Eq. (6). Simulations show that no bias is introduced by this choice and the correct candidate is picked about 88% of the time.

We study various potential sources of background using a combination of Monte Carlo simulation and data events. Two sources of background are identified in large samples of simulated $B\bar{B}$ events. One source is $B^- \rightarrow D^0 K_s^0 \pi^-$ production where the $K_s^0 \pi^-$ is non reso-

nant and has an invariant mass in the K^{*-} mass window. This background is discussed later in this paper. The second background (peaking background) includes instances where a favored decay (e. g. $B^- \rightarrow [K^-\pi^+]_D K^{*-}$) contributes to fake candidates for the suppressed decay (i.e. $B^+ \rightarrow [K^-\pi^+]_D K^{*+}$). The most common way for this to occur is for a π^+ from the rest of the event to be substituted for the π^- in the K^{*-} candidate. Other sources of peaking background include double particle-identification failure in signal events that results in $D^0 \rightarrow K^-\pi^+$ being reconstructed as $D^0 \rightarrow \pi^-K^+$, or the kaon from the D^0 being interchanged with the charged pion from the K^* . We quantify this background with the ratio of the signal efficiency of wrong-sign decay to right-sign decay multiplied by the right-sign yield from data. The total size of this right-sign pollution is estimated to be 2.4 ± 0.3 events. Another class of backgrounds are charmless decays with the same final state as the signal (e.g., $B^- \rightarrow K^{*-}K^+\pi^-$). However, since the branching fraction for many of these charmless decays have not been measured or are poorly measured, we use the D^0 sideband to estimate the contamination from this source. From a fit to the m_{ES} distribution using candidates in the D^0 sideband we find 0.0 ± 1.1 events. We take the 1.1 events as the contribution to the systematic uncertainty from this source.

Signal yields are determined from an unbinned extended maximum likelihood fit to the m_{ES} distribution in the range $5.2 \leq m_{ES} \leq 5.3$ GeV/c^2 . A Gaussian function (\mathcal{G}) is used to describe all signal shapes while the combinatorial background is modeled with an ARGUS threshold function (\mathcal{A}) defined in Eq. (7). The mean and width of the Gaussian as well as the ξ of the ARGUS function are determined by the fit. For a likelihood function we use $a \cdot \mathcal{A} + b \cdot \mathcal{G}$ where a is the number of background events and b the number of signal events. We correct b for the right-sign peaking background previously discussed (2.4 ± 0.3 events).

In Fig. 4 we show the results of a simultaneous fit to $B^- \rightarrow [K^+\pi^-]_D K^{*-}$ and $B^- \rightarrow [K^-\pi^+]_D K^{*-}$ candidates that satisfy all selection criteria. It is in the wrong-sign decays that the interference we study takes place. Therefore in Fig. 5 we display the same fit separately for the wrong-sign decays of the B^+ and the B^- mesons. The results of the maximum likelihood fit are $\mathcal{R}_{ADS} = 0.066 \pm 0.031$, $\mathcal{A}_{ADS} = -0.34 \pm 0.43$, and 172.9 ± 14.5 $B^- \rightarrow [K^-\pi^+]_D K^{*-}$ right-sign events. Expressed in terms of the wrong-sign yield, the fit result is 11.5 ± 5.3 wrong-sign events (3.8 ± 3.4 $B^- \rightarrow [K^+\pi^-]_D K^{*-}$ and 7.7 ± 4.2 $B^+ \rightarrow [K^-\pi^+]_D K^{*+}$ events). The uncertainties are statistical only. The correlation between \mathcal{R}_{ADS} and \mathcal{A}_{ADS} is insignificant.

We summarize in Table IV the systematic uncertainties relevant to this analysis. Since both \mathcal{R}_{ADS} and \mathcal{A}_{ADS} are ratios of similar quantities, most potential sources of systematic uncertainties cancel.

For the estimation of the detection-efficiency asymmetry we use the previously mentioned results from the

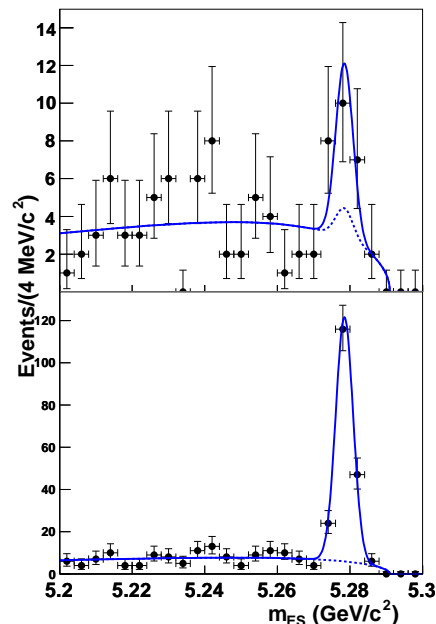


FIG. 4: Distributions of m_{ES} for the wrong-sign (top) and right-sign (bottom) decays. These decay categories are defined in the text. The dashed curve indicates the total background contribution. It also includes the right-sign peaking background estimated from a Monte Carlo study for the wrong-sign (top) decays. The curves result from a simultaneous fit to these distributions with identical PDFs for both samples.

study carried out in [24]. We add linearly the central value and one-standard deviation in the most conservative direction to assign a systematic uncertainty of $\delta A_{ch} = \pm 0.022$ to the \mathcal{A}_{ADS} measurement. To a good approximation the systematic uncertainty in \mathcal{R}_{ADS} due to this source can be shown to be given by $\delta \mathcal{R}_{ADS} = \mathcal{R}_{ADS} \cdot \mathcal{A}_{ADS} \cdot \delta A_{ch}$.

To estimate the systematic uncertainty on \mathcal{A}_{ADS} and \mathcal{R}_{ADS} due to the peaking background, we use the statistical uncertainty on this quantity, ± 0.3 events. With approximately 12 $B^- \rightarrow [K^+\pi^-]_D K^{*-}$ events and 173 $B^- \rightarrow [K^-\pi^+]_D K^{*-}$ events this source contributes ± 0.002 and ± 0.024 to the systematic uncertainties on \mathcal{R}_{ADS} and \mathcal{A}_{ADS} , respectively.

As in Section III, we need to estimate the systematic effect due to the non-resonant $K_S^0\pi^-$ pairs in the K^* mass range. We follow the same procedure discussed in Section III. After adding in quadrature the individual systematic uncertainty contributions listed in Table IV, we find:

$$\begin{aligned} \mathcal{A}_{ADS} &= -0.34 \pm 0.43(\text{stat.}) \pm 0.16(\text{syst.}) \\ \mathcal{R}_{ADS} &= 0.066 \pm 0.031(\text{stat.}) \pm 0.010(\text{syst.}) \end{aligned}$$

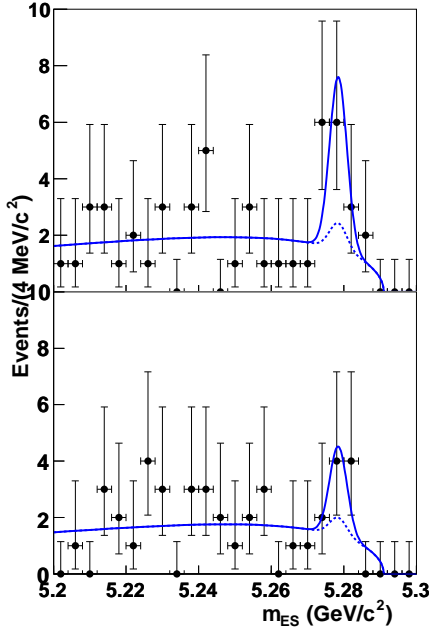


FIG. 5: In this figure the wrong-sign sample shown in the top plot of Fig. 4 is split by charge to measure \mathcal{A}_{ADS} . The upper plot shows the m_{ES} distribution of the $B^+ \rightarrow [K^-\pi^+]_D K^{*+}$ decays while the lower plot presents the same for the $B^- \rightarrow [K^+\pi^-]_D K^{*-}$ decays. The dashed curve indicates the total background contribution which includes the right-sign peaking background estimated from a Monte Carlo study. The curves are the results of the fit.

TABLE IV: Summary of ADS systematic uncertainties.

Source	$\delta\mathcal{R}_{ADS}$	$\delta\mathcal{A}_{ADS}$
Detection asymmetry	± 0.0005	± 0.022
Peaking bkg.	± 0.0020	± 0.024
Same-final-state bkg.	± 0.0061	± 0.091
Non resonant $K_s^0\pi^-$ bkg.	± 0.0073	± 0.126
Total systematic uncertainty	± 0.0097	± 0.159

V. COMBINED RESULTS

We use the GLW and ADS results and a frequentist statistical approach [27] to extract information on r_B and γ . In this technique a χ^2 is calculated using the differences between the measured and theoretical values and the covariance matrix (including systematic errors) of the six measured quantities. The values of r_D and δ_D are taken from Ref. [12], while we allow $0 \leq r_B \leq 1$, $0^\circ \leq \gamma \leq 360^\circ$, and $0^\circ \leq \delta_B \leq 360^\circ$. The minimum of the χ^2 for the r_B , γ , and δ parameter space is calculated first (χ_{\min}^2). We then scan the range of r_B minimizing the χ^2 (χ_m^2) by varying δ and γ . A confidence level for r_B is calculated using $\Delta\chi^2 = \chi_m^2 - \chi_{\min}^2$ and one degree of freedom. We assume Gaussian measurement uncertainties. The results of this procedure are shown in Fig. 6. Com-

binning the ADS and GLW results we find the minimum χ^2 at $r_B = 0.24$ with a one sigma interval of $[0.18, 0.32]$ and a two sigma interval of $[0.11, 0.37]$. We find similar results for r_B using the modifications to this frequentist approach discussed in [28] and using the Bayesian approach of Ref. [29].

Using the above procedure we also find confidence intervals for γ . The results of the scan in γ are shown in Fig. 7. The combined GLW+ADS analysis excludes values of γ in the region $[55, 111]^\circ$ at the one sigma level and $[86, 87]^\circ$ at the two sigma level. The use of the measurement of the strong phase δ_D [12] helps to resolve the ambiguities on γ and therefore explains the asymmetry in the confidence level plot shown in Fig. 7.

In Fig. 8 we show the 95% confidence level contours for r_B versus γ as well as the 68% confidence level contours for the GLW and the combined GLW and ADS analysis (striped areas).

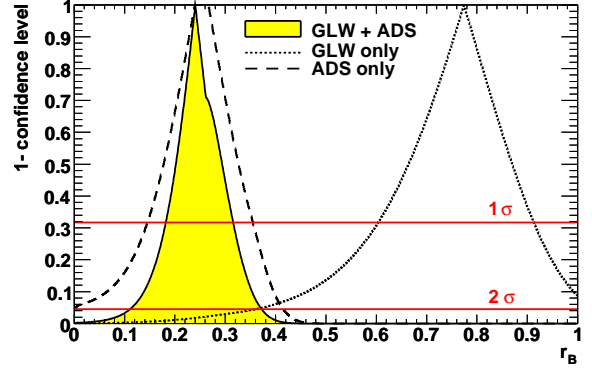


FIG. 6: Constraints on r_B from the combined $B^- \rightarrow D_{CP}K^{*-}$ GLW and ADS measurements. The dashed (dotted) curve shows the 1 minus the confidence level to exclude the abscissa value as a function of r_B derived from the GLW (ADS) measurements. The combined result is given by the solid line and shaded area. The horizontal lines show the exclusion limits at the 1, and 2 standard deviation levels.

VI. SUMMARY

In summary, we present improved measurements of yields from $B^- \rightarrow DK^{*-}$ decays, where the neutral D meson decays into final states of even and odd CP (GLW), and the $K^+\pi^-$ final state (ADS). We express the results as \mathcal{R}_{CP} , \mathcal{A}_{CP} , x_{\pm} , \mathcal{R}_{ADS} and \mathcal{A}_{ADS} . These results in combination with other GLW, ADS, and Dalitz type analyses improve our knowledge of r_B and γ .

VII. ACKNOWLEDGMENTS

We are grateful for the extraordinary contributions of our PEP-II colleagues in achieving the excellent luminos-

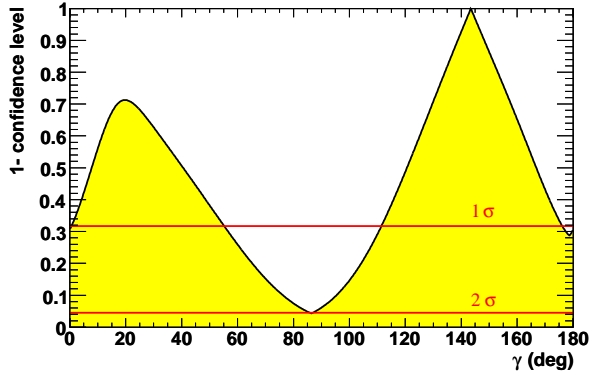


FIG. 7: Constraints on γ from the combined $B^- \rightarrow D_{CP}K^{*-}$ GLW and ADS measurements. The horizontal lines show the exclusion limits at the 1 and 2 standard deviation levels.

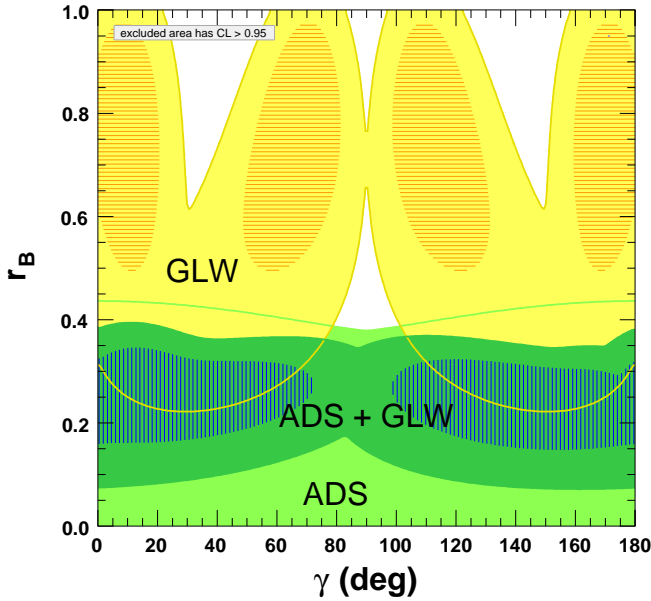


FIG. 8: 95% confidence level contours from a two dimensional scan of γ versus r_B from the $B^- \rightarrow D_{CP}K^{*-}$ GLW and ADS measurements as well as the 68% confidence level regions (striped areas) for the GLW and the combined GLW and ADS results.

594 ity and machine conditions that have made this work possible.
 595 The success of this project also relies critically on
 596 the expertise and dedication of the computing organiza-
 597 tions that support *BABAR*. The collaborating institutions
 598 wish to thank SLAC for its support and the kind hospi-
 599 tality extended to them. This work is supported by the
 600 US Department of Energy and National Science Founda-
 601 tion, the Natural Sciences and Engineering Research
 602 Council (Canada), the Commissariat à l’Energie Atomique
 603 and Institut National de Physique Nucléaire et de
 604 Physique des Particules (France), the Bundesministerium
 605 für Bildung und Forschung and Deutsche Forschungsge-
 606 meinschaft (Germany), the Istituto Nazionale di Fisica
 607 Nucleare (Italy), the Foundation for Fundamental Re-
 608 search on Matter (The Netherlands), the Research Coun-
 609 cil of Norway, the Ministry of Education and Science of
 610 the Russian Federation, Ministerio de Educación y Cien-
 611 cia (Spain), and the Science and Technology Facilities
 612 Council (United Kingdom). Individuals have received
 613 support from the Marie-Curie IEF program (European
 614 Union) and the A. P. Sloan Foundation.

[1] N. Cabibbo, Phys. Rev. Lett. **10**, 531 (1963);
 M. Kobayashi and T. Maskawa, Prog. Theor. Phys. **49**,
 652 (1973).
 [2] “CP Violation”, edited by C. Jarlskog, Advanced Series
 on Directions in High Energy Physics, Volume 3, World
 Scientific (1989).
 [3] C. Amsler *et al.* (Particle Data Group), Phys. Lett. B
667, 1 (2008).

[4] M. Gronau and D. London, Phys. Lett. B **253**, 483
 (1991); M. Gronau, Phys. Rev. D, **58**, 037301 (1998).
 [5] M. Gronau and D. Wyler, Phys. Lett. B **265**, 172 (1991).
 [6] D. Atwood, I. Dunietz, A. Soni, Phys. Rev. Lett. **78**,
 3257 (1997).
 [7] A. Soffer, Phys. Rev. D, **60**, 054032 (1999).
 [8] By D we mean any linear combination of a D^0 and a \bar{D}^0 .
 [9] Hereafter K^{*-} implies $K^*(892)^-$. In this paper we use

- only the $K^{*\pm} \rightarrow K_S^0 \pi^\pm$, $K_S^0 \rightarrow \pi^+ \pi^-$ decay chain.
- [10] J. P. Silva and A. Soffer, Phys. Rev. D **61**, 112001 (2000); Y. Grossman, A. Soffer and J. Zupan, Phys. Rev. D **72**, 031501 (2005).
- [11] A. Giri, Y. Grossman, A. Soffer and J. Zupan, Phys. Rev. D **68**, 054018 (2003).
- [12] E. Barberio et al., “Averages of b-hadron and c-hadron Properties at the End of 2007”, arXiv:0808.1297 and on-line update at http://www.slac.stanford.edu/xorg/hfag/charm/ICHEP08/results_mix+cpv.html
- [13] M. Gronau, Phys. Lett. B **557**, 198 (2003).
- [14] BABAR Collaboration, B. Aubert *et al.*, Phys. Rev. D **72**, 071104 (2005).
- [15] BABAR Collaboration, B. Aubert *et al.*, Phys. Rev. D **72**, 071103 (2005).
- [16] BABAR Collaboration, B. Aubert *et al.*, Nucl. Instr. Methods Phys. Res., Sect. A **479**, 1 (2002).
- [17] GEANT4 Collaboration, S. Agostinelli *et al.*, Nucl. Instr. Methods Phys. Res., Sect. A **506**, 250 (2003).
- [18] D. Lange, Nucl. Instrum. Methods Phys. Res., Sect. A **462**, 152 (2001).
- [19] T. Sjostrand, Comp. Phys. Commun. **82**, 74 (1994).
- [20] BABAR Collaboration, B. Aubert *et al.*, Phys. Rev. D **69**, 032004 (2004).
- [21] BABAR Collaboration, B. Aubert *et al.*, Phys. Rev. Lett. **89**, 281802 (2002).
- [22] G.C. Fox and S. Wolfram, Phys. Rev. Lett. **41**, 1501 (1978).
- [23] ARGUS Collaboration, H. Albrecht *et al.*, Phys. Lett. B **185**, 218, (1987); *ibid.* **241**, 278, (1990).
- [24] BABAR Collaboration, B. Aubert *et al.*, Phys. Rev. D, **77**, 111102 (2008).
- [25] BABAR Collaboration, B. Aubert *et al.*, Phys. Rev. D, **72**, 052008 (2005).
- [26] BABAR Collaboration, B. Aubert *et al.*, Phys. Rev. D **73**, 111104 (2006).
- [27] J. Charles *et al.*, Eur. Phys. J. C **41**,1 (2005).
- [28] BABAR Collaboration, B. Aubert *et al.*, Phys. Rev. D **78**, 034023 (2008).
- [29] M. Ciuchini *et al.*, JHEP **507**, 28 (2005).